Surface properties of 3d transition metals

Marko P J Punkkinen, Qing-Miao Hu, Se Kyun Kwon, Borje Johansson, János Kollár, Levente Vitos

Surface properties of 3d transition metals

Journal:	*Philosophical Magazine & Philosophical Magazine Letters*
Manuscript ID:	TPHM-11-Feb-0082.R1
Journal Selection:	Philosophical Magazine
Date Submitted by the Author:	06-May-2011
Complete List of Authors:	Punkkinen, Marko; Royal Institute of Technology, Department of Materials Science and Engineering; University of Turku, Department of Physics and Astronomy Hu, Qing-Miao; Institute of Metal Research, Chinese Academy of Sciences, Shenyang National Laboratory for Materials Sciences Kwon, Se Kyun; Pohang University of Science and Technology, Graduate Institute of Ferrous Technology Johansson, Borje; Condensed Matter Theory Group, Department of Physics Kollár, János; MTA SZFKI Vitos, Levente; MTA SZFKI
Keywords:	surface properties, density-functional methods, magnetism
Keywords (user supplied):	surface energy, surface stress, magnetic transition metals

Philosophical Magazine
Vol. 00, No. 00, 00 Month 2011, 1–13

Surface properties of $3d$ transition metals

M.P.J. Punkkinen[a,b], Q.-M. Hu[c], S.K. Kwon[d], B. Johansson[a,e], J. Kollár[f†], and L. Vitos[a,e,f*]

[a]*Applied Materials Physics, Department of Materials Science and Engineering, Royal Institute of Technology, SE-100 44 Stockholm,Sweden*; [b]*Department of Physics and Astronomy, University of Turku, FI-20014 Turku, Finland*; [c]*Shenyang National Laboratory for Materials Sciences, Institute of Metal Research, Chinese Academy of Sciences, 72 Wenhua Road, Shenyang 110016, China*; [d]*Graduate Institute of Ferrous Technology, Pohang University of Science and Technology, Pohang 790-784, Korea*; [e]*Department of Physics and Materials Science, Uppsala University, SE-75120 Uppsala, Sweden*; [f]*Research Institute for Solid State Physics and Optics, H-1525 Budapest, P.O.Box 49, Hungary*

(*28 February 2011*)

Using the projector augmented wave method within density functional theory, we present a systematic study of the layer relaxation, surface energy and surface stress of $3d$ transition metals. Comparing the calculated trends for the surface energy and stress with those obtained for $4d$ and $5d$ metals we find that magnetism has a significant effect on the surface properties. Enhanced surface magnetic moments decrease the size of the surface relaxation, lower the surface energy and surface stress, leading to compressive stress in Cr and Mn.

Keywords: surface relaxation; surface energy; surface stress; magnetic transition metals; density functional theory

1. Introduction

Surface energy (γ) and surface stress (τ_{ij}) are two fundamental physical parameters of surfaces. For solids, they differ by the excess or residual surface stress $\tau_{ij}-\gamma\delta_{ij} = \partial\gamma/\partial\epsilon_{ij}$, where ϵ_{ij} stands for the strain within the surface plane. For high symmetry surfaces, often the scalar surface stress is used (τ), which corresponds to the average stress along in-plane directions. For liquids, the surface free energy and the surface stress are equal each other due to the fact that in this case the surface energy does not change when the surface is strained, *i.e.* $\partial\gamma/\partial\epsilon = 0$.

Knowledge of the geometry of solid surfaces is amongst the basic questions of surface science. This is because in general the surface parameters exhibit strong structure dependence [1]. Transition metal surfaces are of particular interest, since they act as catalysts in various chemical reactions. It is well known that real surfaces of pure metals can adopt different structures from those of ideally truncated crystals. Upon layer relaxation only rigid inward or outward displacement of the atomic layers occurs, while in case of reconstruction, the displacement of atoms may alter the two-dimensional symmetry of the surface. Experimental studies have

†Deceased.

*Corresponding author. Email: levente@kth.se

ISSN: 1478-6435 print/ISSN 1478-6443 online

DOI: 10.1080/14786435.20xx.xxxxxx
http://www.informaworld.com

demonstrated that the surface layer of clean transition metal surfaces relaxes inward [2], *i.e.* the inter-layer distance between the topmost two atomic layers is smaller than that of the bulk. Outward expansion of the top layer has also been found for some surfaces of noble metals. The top layer relaxation is often accompanied by relaxation of the subsurface atomic layers, resulting in an oscillatory behavior of multi-layer relaxation.

Several theoretical models have been proposed to explain the surface relaxation of transition metals. Generally, the magnitude of relaxation is larger for rough surfaces than for smooth ones. The model, proposed by Finnis and Heine [3] based on Smoluchowski smoothing [4], states that when cutting a perfect crystal, charge redistribution gives rise to an inward electrostatic force on the top layer nuclei. Since this effect increases with surface roughness, the above model confirms the general relationship between relaxation and surface roughness. It also explains the contraction found for most transition metal surfaces, but it fails to describe the noble metal surface relaxation. Pettifor [5] suggested that the crystal geometry is determined by the balance of the negative pressure of the localized d bonds and the homogeneous positive pressure of the sp electrons. According to Heine and Marks [6], at metal surfaces the mobile sp electrons can flow into the vacuum, while the d bonds between the first and second layers remain practically unchanged. Therefore, the d electrons give rise to an inward force on the surface atoms, which is proportional to the strength of the d bonds. Because the strength of the d bonds shows a well known parabolic behavior across the transition metal series, the magnitude of the top layer relaxation is also expected to follow a parabolic trend. This model predicts positive (outward) relaxation for noble metal surfaces. A third approach, introduced by Kádas et al. [7] using *ab initio* results based on the exact muffin-tin orbitals method [8, 9], gives a quantitative foundation for the model by Heine and Marks. According to that, the layer relaxation (δ) is proportional to $(V/B)\Delta n_{sp}$, where Δn_{sp} is the depletion of sp electrons in the surface layer relative to bulk, V and B are the atomic volume and bulk modulus. Since Δn_{sp} follows a parabolic trend across the nonmagnetic transition series [7] the above expression would indeed dictate a parabolic shape for δ as a function of d-occupation number. However, due to the large equilibrium volume and the rather small bulk modulus of the early transition metals, the multiplier V/B is relatively large at the beginning of the series resulting in large layer relaxations for those elements.

One possible way to approach the problem of surface relaxation is to treat the surface as a two-dimensional defect with a potential which is screened towards the bulk metal. It is well known that free surfaces cause Friedel oscillations in the charge density towards the bulk metal [10]. The periodicity of the Friedel oscillation is twice the Fermi wave vector k_F and it is generally incommensurate with the relevant lattice constant (inter-layer distance) of the metal. This causes the layer relaxation to fall off quickly towards the bulk. However, if the lattice constant and $2k_F$ are commensurate, then the layer relaxation and the Friedel oscillation strengthen each other, which results in a slowly decaying layer relaxation towards the bulk. Striking examples are the hexagonal close-packed Tc and Re [1, 11, 12], where the magnitude of the deep layer relaxations were found to be similar to those of the top-layers.

Both the surface energy and surface stress are sensitive to the actual surface geometry. In particular, the layer relaxation dependence of the surface stress is closely linear whereas that of the surface energy quadratic [1]. Due to the linear term, any accurate surface stress calculation must be preceded by a precise surface geometry study. Kwon *et al.* [1] connected the layer relaxation dependence of γ and τ to the surface elastic constants. Nichols *et al.* [13] explained the surface stress

change during surface relaxation in terms of a jellium model.

According to a simple model described by Ibach [14], upon cleaving a metal surface the electronic charge density of the broken bonds is redistributed between surface atoms and their backbonds. Hence, surfaces should possess inward layer relaxation as a result of the strengthening of the backbonds of surface atoms. On the other hand, since lattice constraint by sub-surface layers hinders in-plane relaxation of surface atoms, the increased charge density between surface atoms is expected to result in tensile (positive) surface stress on metal surfaces. First-principles calculations performed for non-magnetic transition metals [1, 11, 15] indeed confirmed that the surface stress on clean metal surfaces is tensile. However, a recent density functional study on $3d$ metals [16] demonstrated that magnetism can overwrite this normal behavior in magnetic transition metals resulting in compressive surface stress for some of the close-packed surfaces. The atomic-scale mechanism behind this anomalous surface stress has been shown to be the enhanced magnetism near the free surfaces, which favors a larger lattice constant as compared to the bulk. In this paper, we provide further details of our study performed for $3d$ metals [16] by presenting *ab initio* data on the top layer relaxation, surface energy and surface stress. In Section 2 we outline the method of the surface energy and stress calculation, while in Section 3 we summarize and discuss the results.

2. Computational method

2.1. *Surface energy and stress*

The surface stress is defined to be the reversible work per unit area to stretch the surface elastically. It can be expressed by the Shuttleworth equation [17]

$$\tau_{ij} = \frac{1}{A}\frac{\partial A\gamma}{\partial \varepsilon_{ij}} = \gamma\delta_{ij} + \frac{\partial \gamma}{\partial \varepsilon_{ij}}, \tag{1}$$

where τ_{ij} denotes the components of the surface stress tensor, A is the surface area, ε_{ij} stands for a deformation tensor element, γ denotes the surface energy, and δ_{ij} is the Kronecker delta. The surface energy is defined as the reversible work per surface area to create a surface, and may be determined as

$$\gamma = \frac{E^s - E^b}{A}, \tag{2}$$

where E^s is the total energy of the surface region and E^b is the total energy of a bulk region, both of them referring to the same number of atoms. Throughout the paper, upper s index refers to surface and upper b index to bulk quantities. In equations (1) and (2), all quantities are evaluated for the unstrained lattice, *i.e.* for $\varepsilon_{ij} = 0$. Since around the equilibrium, the variation of the bulk energy $E^b(\varepsilon)$ as a function of lattice strain vanishes in linear order, in fact it is the linear strain dependence of $E^s(\varepsilon)$ that leads to nonzero stress.

A general expression of the layer relaxation dependence of the above surface parameters may be formulated as follows. Here for the sake of simplicity we assume that only the top layer is relaxed, *viz.* there is only one inter-layer distance λ different from the ideal bulk value. Using notation ε for the biaxial in-plane strain [15, 18] and $\delta = (\lambda - \lambda_0)/\lambda_0$ for the deviation relative to the equilibrium (surface

or bulk) inter-layer separation λ_0, the fully relaxed slab energy relative to the bulk energy can formally be expanded as

$$E^s(\varepsilon,\delta) - E^b(\varepsilon,\delta) \sim E^s(0,0) - E^b(0,0) + \\ + A_0\left(\tau_0\varepsilon + \frac{1}{2}\gamma_\varepsilon\varepsilon^2 + \frac{1}{2}\gamma_\delta\delta^2 + \tau_0^{'}\varepsilon\delta + ...\right), \quad (3)$$

where $\tau_0, \gamma_\varepsilon, \gamma_\delta$ and $\tau_0^{'}$ are constants and A_0 is the area of the undistorted surface. Note that in expansion (3) the pure linear term in δ vanishes because the slab energy corresponds to the layer relaxed structure (*viz.* $\partial E^s(\varepsilon=0,\delta)/\partial\delta = 0$ for $\delta = 0$) and the bulk energy $E^b(\varepsilon,\delta)$ contains only second and higher order terms in δ and ε. Using the above expression in connection with definitions (1) and (2), in the limit $\varepsilon \to 0$ we find

$$\gamma(\delta) = \gamma(0) + \frac{1}{2}\gamma_\delta\delta^2 + ... \quad (4)$$

and

$$\tau(\delta) = \tau(0) + \tau_0^{'}\delta + ..., \quad (5)$$

where $\gamma(0) = (E^s(0,0) - E^b(0,0))/A_0$ and $\tau(0) = \tau_0$. Equations (4) and (5) are equivalent to those derived by Kwon *et al.* [1]. According to these expressions, the surface energy depends on the layer relaxation only in the second order but the surface stress due to the mixed term in (3) exhibits a much stronger δ dependence.

2.2. *Numerical details*

In order to calculate the surface stress, we consider a slab formed by N atomic layers parallel to the surface. For surface calculations, the slab is embedded in vacuum, while for bulk calculations the slab is periodically repeated along the direction perpendicular to the atomic layers. The bulk is relaxed to its equilibrium with equilibrium inter-layer distance λ_0. Next, for the slab with in-plane lattice parameters fixed to those of the bulk, we perform multi-layer relaxation (apart from a few central layers, where the inter-layer distance is kept at λ_0) and find the λ inter-layer distances which minimize the total slab energy. In other words, the only allowed relaxation is the one which is perpendicular to the surface plane, i.e. we do not consider in-plane relaxation. Starting from the so relaxed slab geometry, we elongate the lattice vectors lying in the surface plane by ε but keep the inter-layer distances fixed. For this distortion, the deformation tensor has the form

$$\varepsilon_{ij} = \begin{bmatrix} \varepsilon & 0 & 0 \\ 0 & \varepsilon & 0 \\ 0 & 0 & 0 \end{bmatrix}. \quad (6)$$

The total energies of the surface and bulk slabs, *i.e.* E^s and E^b, are computed for five different deformations ($\varepsilon = 0$, ± 0.01 and ± 0.02) and fitted by a quadratic polynomial, *i.e.*

$$E^{s/b}(\varepsilon) \approx E^{s/b}(0) + c_1^{s/b}\varepsilon + c_2^{s/b}\varepsilon^2. \quad (7)$$

Here $E^b(0)$ is the total energy of the undistorted bulk and $E^s(0)$ is the total energy of the undistorted slab (corresponding to $\delta = 0$). The surface stress is determined from the linear coefficients of the slab and bulk energies at $\varepsilon = 0$ (unstrained lattice), *viz.*

$$\tau = \frac{c_1^s - c_1^b}{4A}, \quad (8)$$

where the factor 4 arises from the two surfaces of the slab and the two deformed in-plane lattice vectors. In the case of low symmetry surfaces, equation (8) gives the average of the two main stress tensor components. Obviously, at equilibrium the bulk stress should vanish ($c_1^b = 0$) and thus it is expected that the surface stress reduces to $c_1^s/(4A)$. However, due to different numerical parameters in bulk and slab calculations, this is not always the case and thus equation (8) is recommended in stress calculations based on the total energy.

In the present application, the free surfaces were modeled by periodically repeated slabs separated by vacuum layers. At ambient conditions, V and Fe have the body centered cubic (bcc) structure; Sc, Ti, Co and Zn have the hexagonal close-packed (hcp) structure, and Ni and Cu are face centered cubic (fcc) metals. Chromium has an incommensurable antiferromagnetic state, which however can be approximated by a commensurable antiferromagnetic state with B2 structure [19]. In the following, when referring to bcc Cr we mean in fact B2 Cr. The ferromagnetic state was used for Fe, Co and Ni. For each system, the surface properties were computed for the most stable facet and for some systems also for the second most stable facet. The slabs were formed by 8 atomic layers for the fcc (111) and (100) surfaces, 12 atomic layers for the bcc (110) and hcp (0001) surfaces, and 16 atomic layers for the bcc (100) surface. For these systems, the thickness of the vacuum layer was set to $22 - 23$ Å. Manganese adopts a complex antiferromagnetic structure (α-Mn) with 58 atoms in the unit cell. The (110) facet of α-Mn was reported to be the most stable surface [20]. This surface was modeled by a slab containing 130 Mn atoms separated by a vacuum layer of thickness 12.2 Å.

All numerical calculations were performed using density functional theory [21] in combination with the generalized gradient approximation [22]. The surface geometry, surface energy, and surface stress were computed using the projector augmented wave (PAW) method as implemented in the Vienna Ab initio Simulation Package (VASP) [23, 24]. In addition to the PAW calculations, we also carried out a series of tests for the unrelaxed bcc (001) surfaces of V, Cr, Mn and Fe. In these tests we employed two alternative *ab initio* total energy approaches. The first tool is based on the exact muffin-tin orbitals (EMTO) method [8, 9, 25, 26] and the second one on the full-potential augmented plane wave with local orbitals (FP APW+lo) method as implemented in WIEN2k package [27, 28].

The EMTO method [26] is a screened Korringa-Kohn-Rostoker type of method [29–31]. In the present application the one-electron Kohn-Sham equation is solved within the scalar-relativistic approximation (omitting the spin-orbit term) and using the Green's function technique. The one-electron potential is represented by optimized overlapping muffin-tin potential spheres. By using overlapping spheres, one describes more accurately the exact crystal potential, compared to the conventional muffin-tin or non-overlapping approach [25, 32]. In combination with the

Table 1. Calculated bulk lattice parameters (in Å) and optimized c/a ratios for the 3d metals. For comparison, the experimental data are given in parentheses [48, 49].

Metal	Structure	a	c/a
Sc	hcp	3.32 (3.31)	1.55 (1.59)
Ti	hcp	2.94 (2.95)	1.59 (1.59)
V	bcc	2.99 (3.03)	
Cr	bcc[a]	2.87 (2.88)	
Mn	bcc[b]	2.80	
	α-Mn	8.64 (8.88)	
Fe	bcc	2.84 (2.87)	
Co	hcp	2.49 (2.51)	1.62 (1.62)
Ni	fcc	3.52 (3.52)	
Cu	fcc	3.64 (3.61)	
Zn	hcp	2.66 (2.66)	1.86 (1.86)

[a]commensurable antiferromagnetic state with B2 structure [19].
[b]hypotetical ferromagnetic structure.

full charge density technique [33–35] for the total energy calculation [9, 25], the EMTO method is also suitable to describe accurately the total energy with respect to anisotropic lattice distortions. The EMTO method has been applied successfully in the theoretical study of the thermophysical properties of metallic alloys [9, 25, 36–41] and complex oxides [42–45]. The FP APW+lo method treats the potential and charge density without any shape-approximations inside the muffin-tin spheres and in the interstitial region [46]. The wave-function is expressed as the augmented plane wave (APW) plus local orbitals for the semicore states [28]. The APW with each radial wave function is computed at a fixed linearization energy. The local orbitals are evaluated at the same energy as the APW's and vanish at the muffin-tin boundary. The APW+lo scheme leads to significantly smaller basis sets and therefore reduces the computation time as compared to the linearized augmented plane wave method without losing accuracy.

In PAW calculations, for all slabs, the in-plane lattice constant was fixed to the theoretical bulk equilibrium value, and the inter-layer distances, except for the central layers, were allowed to relax to their equilibrium values. The optimization of the atomic structure was performed using conjugate-gradient minimization of the total energy with respect to the atomic coordinates. The atoms were relaxed until the remaining forces were less than 20 meV/Å. The Brillouin zone sampling was performed by the Monkhorst-Pack scheme [47]. The chosen plane wave cut-off energy (450-500 eV) in PAW calculations and the k-mesh in EMTO and FP APW+lo calculations assured ~ 1 meV per atom convergence in the total energy. For each surface, the mean surface stress was determined from the variation of the surface energy upon biaxial in-plane strain [15, 18].

3. Results and discussion

3.1. *Layer relaxation*

The calculated bulk equilibrium lattice parameters and c/a-ratios for the 3d metals including Zn are listed in Table 1. They are in good agreement with former theoretical results obtained using the same exchange-correlation functional [50] as well as with the quoted experimental data [48, 49].

In Table 2, we give our results for the multi-layer relaxation obtained for some low-index surfaces of 3d transition metals. Examining the layer relaxations, we

Table 2. Calculated layer relaxations (in percent) for some low-index surfaces of 3*d* transition metals. In the case of Mn, the numbers in parenthesis represent the relaxations for the first two close-packed layers, *viz.* δ_{13} and δ_{34}.

	Surface	Relaxation		
		δ_{12}	δ_{23}	δ_{34}
Sc	hcp(0001)	-2.58	1.19	0.29
Ti	hcp(0001)	-7.14	2.87	-0.49
V	bcc(100)	-12.41	0.24	2.87
	bcc(110)	-5.24	0.58	0.01
Cr	bcc(100)	-5.06	3.62	-1.04
	bcc(110)	-1.95	0.44	0.20
Mn	α(110)	-6.95	12.30	-1.83
		(0.99)		(-1.83)
Fe	bcc(100)	-0.18	2.88	0.78
	bcc(110)	-0.05	0.71	-0.15
Co	hcp(0001)	-2.89	1.85	-0.72
Ni	fcc(100)	-3.74	0.55	0.04
	fcc(111)	-1.31	-0.09	0.11
Cu	fcc(100)	-1.61	1.48	1.25
	fcc(111)	-0.31	0.04	0.31
Zn	hcp(0001)	0.69	-0.65	-0.10

see that for most 3*d* metals the relaxation decays relatively fast with the distance from the surface. For most of the systems, especially where the expected crystal structure is not altered by magnetic effects, the top layer relaxation follows similar trend as those observed for the 4*d* and 5*d* metals [11]. Exceptions are the bcc (110) surfaces of Cr and Fe, where the calculated relaxations of -1.95 % and -0.05 % are significantly smaller than those obtained for the other metals from the same groups. In particular, for the top layer relaxation of the close-packed surfaces of W and Os, Zolyomi *et al.* [11] predicted -3.76 % and -3.72 %, respectively, whereas for Mo and Ru Kwon *et al.* [1] obtained -4.74 % and -3.96 %, respectively. Note that the same is true for the bcc (100) surface of Cr when compared to that of Mo or W [1, 11]. Manganese is a somewhat special case. If atomic layers are defined for the (110) surface of α-Mn, there will be a less dense layer between the first two relatively close-packed layers. The inter-layer distance between this loosely packed second layer and the third layer is small, which explains the large δ_{23} from Table 2. Omitting this less dense layer, the first two inter-layer separations for α-Mn relax by $\delta_{13} = 0.99\%$ and $\delta_{34} = -1.83\%$, respectively. These figures are close to those obtained for Cr and Fe. Thus, according to the present *ab initio* calculations, the close-packed surfaces of the magnetic 3*d* metals show unusually small layer relaxation. We suggest that the relatively small surface relaxation obtained for some of the magnetic metals is attributed to the positive magnetic pressure around the free surfaces (see Section 3.3).

3.2. *Surface energy*

The calculated surface energy, stress, and excess surface stress are listed in Table 3 for some low index surfaces of 3*d* transition metals. For the thermodynamically stable surfaces, the present surface energies (γ_{3d}) are compared to those obtained for the 4*d* (γ_{4d}) and 5*d* (γ_{5d}) metals in Figure 1. We observe that the three transition metal series possess rather similar surface energies both in magnitude and in trend as a function of *d*-occupation. This similarity is even more interesting if

Table 3. Calculated surface energy (γ), total (τ) and excess ($\tau - \gamma$) surface stress (in J/m^2) for 3d transition metals. The results correspond to the fully layer-relaxed geometry (except bcc Mn, where the ideal unrelaxed geometry was used).

	Surface	γ	τ	$(\tau - \gamma)$
Sc	hcp(0001)	1.26	0.73	-0.53
Ti	hcp(0001)	1.97	0.65	-1.32
V	bcc(100)	2.40	2.12	-0.28
	bcc(110)	2.41	2.12	-0.29
Cr	bcc(100)	3.06	-0.32	-3.38
	bcc(110)	3.10	0.79	-2.31
Mn	bcc(100)	2.14	-2.24	-4.38
	α(110)	2.59	-0.22	-2.81
Fe	bcc(100)	2.50	1.39	-1.11
	bcc(110)	2.45	1.56	-0.89
Co	hcp(0001)	2.11	2.20	0.09
Ni	fcc(100)	2.22	1.73	-0.49
	fcc(111)	1.92	2.16	0.24
Cu	fcc(100)	1.44	2.55	1.11
	fcc(111)	1.30	1.87	0.57
Zn	hcp(0001)	0.32	1.44	1.12

we realize that there are differences in the morphology of the most stable surfaces. For instance, Cr has as the most stable surface the bcc (100) facet compared to the bcc (110) facet of Mo and W. All three bcc metals from the Cr group possess the largest surface energy across the transition series.

The local maximum (minimum) seen for Ru and Os (Tc and Re) is missing from γ_{3d}. However, this deviation may be ascribed to the complex crystallographic structure of α-Mn. Indeed, the surface energies calculated for the hypothetical bcc (100) facet show a shallow minimum around Mn. These results were obtained for the unrelaxed bcc (100) surface and are shown in Figure 2. We find that all three *ab initio* methods (PAW, EMTO and FP APW+lo) give the same surface energy trends as going from V to Fe.

For illustration of the magnetic contribution in the surface energy, Figure 2 displays also the bcc (100) surface energies obtained from nonmagnetic PAW and EMTO calculations. Clearly, there is a large drop in the surface energy of bcc Mn due to the magnetism: 1.200 J/m^2 calculated in PAW and 1.102 J/m^2 in EMTO. The magnetic effect is somewhat smaller for Cr and Fe: 0.750 J/m^2 and 0.490 J/m^2 in PAW (0.529 J/m^2 and 0.746 J/m^2 in EMTO).

Another important feature of the theoretical data from Figure 2 is that in all three calculations and for both magnetic states, the surface energy of Cr turns out to be larger than that of bcc V. This might be in apparent contradiction with previous theoretical calculations based on the linear muffin-tin orbitals method [51, 52]. However, if we consider the same bcc (100) or bcc (110) crystallographic facets for V and Cr, then the four sets of theoretical results are consistent with each other. Interestingly, none of the theoretical set of results confirms the experimental estimate by Tyson and Miller [53], as it was inspired in Ref. [51]. The estimated surface energies (γ_{3d}^{est}) for V, Cr, Mn, and Fe are 2.62, 2.35, 1.54, and 2.42 J/m^2, respectively. The deep local minimum in these "experimental" surface energies is absent from γ_{3d} from Figures 1 and 2. Although theory might predict a weak local minimum in γ_{3d} near Mn when calculating for the same crystallographic facet (bcc (100), Figure 2), this theoretical minimum is much shallower than that in γ_{3d}^{est}. Using continuum model approach [54], Punkkinen *et al.* [16] demonstrated that

the deep minimum in the estimated surface energies for bcc $3d$ metals is, to a large extent, a consequence of the compressive surface stress of Cr and Mn (see Section 3.3).

3.3. *Surface stress*

For the thermodynamically stable surfaces, the present surface stresses (τ_{3d}) are compared to those obtained for the $4d$ (τ_{4d}) and $5d$ (τ_{5d}) metals in Figure 3. While τ_{4d} and τ_{5d} are relatively similar, we observe that τ_{3d} exhibits a rather different behavior as a function of d-occupation (N_d). For $N_d \leq 3$ and $N_d \geq 7$ the present τ_{3d} and $(\tau_{3d} - \gamma_{3d})$ follow similar trends as those calculated for the $4d$ and $5d$ metals. However, for Cr, Mn and Fe we can see a deep minimum in τ_{3d}. Most surprisingly, for Cr and Mn the surface stress of the thermodynamically most stable surfaces becomes compressive: -0.32 J/m^2 for Cr and -0.22 J/m^2 for Mn. That is, the thermodynamically stable surfaces of Cr and Mn prefer a larger lattice constant than their bulk counterparts. Apparently, these two systems are the only transition metal surfaces where the Ibach's model fails.

Recently, we demonstrated that the marked deviation between τ_{3d} and its $4d$ and $5d$ counterparts is due to the enhanced surface magnetism in Cr, Mn, Fe, Co and Ni as compared to their bulk [16]. We define the magnetic contribution to the surface stress (τ^m) as the difference between the nonmagnetic (NM) and magnetic (Mag) values. It turns out that the magnetic surface stress for Cr, Mn, and Fe is of order of the corresponding NM surface stress. Namely, $\tau^m_{\rm Cr} = 5.41$ Jm^{-2} (102% of NM $\tau_{\rm Cr}$), $\tau^m_{\rm Mn} = 5.00$ Jm^{-2} (99%) and $\tau^m_{\rm Fe} = 3.88$ Jm^{-2} (71%). That is, surface magnetism drastically reduces the surface stress of Cr, Mn and Fe. For Co and Ni we have somewhat smaller magnetic effects, $\tau^m_{\rm Co} = 1.11$ Jm^{-2} (30%) and $\tau^m_{\rm Ni} = 0.44$ Jm^{-2} (15%).

In order to visualize the impact of magnetism on the surface stress, we realize that the decrease of the surface stress is associated with the excess magnetic pressure (P_{mag}) around the free surface. For $3d$ itinerant ferromagnetic systems, using the Stoner model and the atomic sphere approximation, we can estimate the magnetic pressure contribution relative to the non-polarized case as [55]

$$3P_{mag}V = -\mu^2 I \Delta_d S^2 + \alpha \Delta E(\mu) \tag{9}$$

where I, Δ_d, S stand for the Stoner exchange parameter, the width of the $3d$ band, and the atomic radius, respectively. The band energy change with respect to the non-polarized value, belonging to the actual value of the magnetic moment μ is denoted by $\Delta E(\mu)$. The parameter α characterizes the decrease of the d-band width Δ_d with increasing volume

$$\alpha = -\frac{\partial ln \Delta_d}{\partial ln S}. \tag{10}$$

Here the symbol ∂ indicates a restricted variation during volume change (the potential is kept frozen [55]). Similarly, using these quantities we can express the energy change during spin polarization as

$$E_{mag} = -\frac{1}{4}\mu^2 I + \Delta E(\mu). \tag{11}$$

In leading order in μ^2 we have

$$\Delta E(\mu) \sim \frac{\mu^2}{4N(\epsilon_F)}, \tag{12}$$

so the magnetic energy becomes

$$E_{mag} \sim \frac{\mu^2}{4N(\epsilon_F)} \left[1 - IN(\epsilon_F)\right]. \tag{13}$$

When the Stoner condition is satisfied, *i.e.* $IN(\epsilon_F) > 1$, E_{mag} is always negative, as it should be. Finally, for the leading term in the pressure we obtain

$$3P_{mag}V \sim \frac{\mu^2 \Delta_d S^2}{N(\epsilon_F)} \left[\frac{\alpha}{4\Delta_d S^2} - IN(\epsilon_F)\right]. \tag{14}$$

For the $3d$ elements where magnetism occurs from Cr to Ni the values of the α parameter lies between 4 and 5, and thus the first term in the expression of $3P_{mag}V$ is typically 10 (usually lies between 8 an 11). This should be compared with the values of $IN(\epsilon_F)$, which is the largest for bcc Fe when equals to 2 and usually lies between 1 and 2. Thus we can generally say that the first term in equation (14) is roughly an order of magnitude larger than the second, which means that the magnetic pressure contribution for these elements is always positive.

Due to the reduced coordination, the surface magnetization is generally enhanced compared to the bulk value, resulting in larger surface magnetic moment (μ_s) than the bulk counterpart (μ_b). Hence, according to equation (14), an excess surface magnetic pressure should appear near free surfaces. Assuming that this excess surface pressure is responsible for the magnetic surface stress, we arrive at $\tau^m \sim \Delta\mu^2$, where $\Delta\mu^2 \equiv \mu_s^2 - \mu_b^2$ represents the surface induced enhancement of the square of the magnetic moment. Punkkinen *et al.* [16] confirmed the almost perfectly linear relationship between τ^m and $\Delta\mu^2$. Therefore, we can conclude that the enhanced surface magnetism is the primary factor responsible for the unusually small or negative surface stress of the magnetic $3d$ metals. Another consequence of the positive surface magnetic pressure is the unusually small surface relaxation obtained for Cr and Fe (and to some extent also Mn).

4. Conclusions

We have presented a systematic theoretical study of the layer relaxation, surface energy, and surface stress of $3d$ transition metals, and examined the atomic number dependence of the above surface parameters. In addition, we have pointed out the unusually small surface relaxation for some of the magnetic metals, and the exceptionally low excess surface stress in the middle of the series. Finally, we have demonstrated that the revealed anomalous trends are the consequence of the enhanced surface magnetism experienced first of all in Cr, Mn and Fe.

5. Acknowledgments

The Swedish Research Council, the Swedish Foundation for International Cooperation in Research and Higher Education (STINT), the Swedish Steel Producer's Association, the Carl Tryggers Foundation, the National Research Foundation of Korea (KSRCP-2008-08) and the Hungarian Scientific Research Fund (research projects OTKA 84078 and K77771-IN83114) are acknowledged for financial support. The calculations were performed at the Finnish IT Center for Science.

References

[1] S.K. Kwon, Z. Nabi, K. Kádas, L. Vitos, J. Kollár, B. Johansson and R. Ahuja, Phys. Rev. B, 72 (2005) 235423.
[2] W. Martienssen and H. Warlimont, Springer Handbook of Condensed Matter and Materials Data, Springer, 2005.
[3] M.W. Finnis and V. Heine, J. Phys. F 4 (1974) L37.
[4] R. Smoluchowski, Phys. Rev. 60 (1941) 661.
[5] D.G. Pettifor, J. Phys. F 8 (1978) 219.
[6] V.Heine and L.D. Marks, Surf. Sci. 165 (1986) 65.
[7] K. Kádas, Z. Nabi, S. K. Kwon, L. Vitos, R. Ahuja, B. Johansson, and J. Kollár, Surf. Sci. 600 (2006) 395.
[8] L. Vitos, H. L. Skriver, B. Johansson, and J. Kollár, Comp. Mat. Sci. 18 (2000) 24.
[9] L. Vitos, Phys. Rev. B 64 (2001) 014107.
[10] J.-H. Cho, Ismail, Z.Zhang, E. W.Plummer, Phys. Rev. B59 (1999) 1677.
[11] V. Zólyomi, L. Vitos. J. Kollár, Phys. Rev. B 78 (2008) 195414.
[12] V. Zólyomi, J. Kollár, L. Vitos, Philosophical Magazine 88, (2008) 2709.
[13] R.J. Nichols, T. Nouar, C.A. Lucas, W.Haiss and W.A. Hofer, Surf. Sci. 513 (2002) 263.
[14] H. Ibach, Surf. Sci. Rep. 29 (1997) 193.
[15] J. Kollár, L. Vitos, J.M. Osorio-Guillén and R. Ahuja, Phys. Rev. B 68 (2003) 245417.
[16] M. P. J. Punkkinen, S. K. Kwon, J. Kollár, B. Johansson, and L. Vitos, Phys. Rev. Lett. 106 (2011) 057202.
[17] R. Shuttleworth, Proc. Phys. Soc. A 63 (1950) 445.
[18] Tong-Yi Zhang, Zhi-Jia Wang, and Wing-Kin Chan, Phys. Rev. B 81 (2010) 195427.
[19] R. Hafner, D. Spisak, R. Lorenz, and J. Hafner, Phys. Rev. B 65 (2002) 184432.
[20] T. F. Liu and J. C. Tasy, Scripta Met. 21 (1987) 1213.
[21] P. Hohenberg and W. Kohn, Phys. Rev. B 136 (1964) 864.
[22] J.P. Perdew, K. Burke, and M. Ernzerhof, Phys. Rev. Lett. 77 (1996) 3865.
[23] P. E. Blöchl, Phys. Rev. B 50 (1994) 17953; G. Kresse and D. Joubert, Phys. Rev. B 59 (1999) 1758.
[24] G. Kresse and J. Hafner, Phys. Rev. B 47 (1993) 558; G. Kresse and J. Hafner, Phys. Rev. B 49 (1994) 14251; G. Kresse and J. Furthmüller, Comput. Mat. Sci. 6 (1996) 15; G. Kresse and J. Furthmüller, Phys. Rev. B 54 (1996) 11169.
[25] L. Vitos, *Computational Quantum Mechanics for Materials Engineers* (Springer-Verlag, London, 2007).
[26] O. K. Andersen, O. Jepsen, and G. Krier, in *Lectures on Methods of Electronic Structure Calculations*, edited by V. Kumar, O. K. Andersen, and A. Mookerjee (World Scientific, Singapore 1994), pp. 63-124.
[27] K. Schwarz, P. Blaha, and G.K.H. Madsen, Comp. Phys. Comm. 147 (2002) 71.
[28] E. Sjstedt, L. Nordström, and D.J. Singh, Solid State Comm. 114 (2000) 15.
[29] J. Korringa, Physica 13 (1947) 392; W. Kohn, and N. Rostoker, Phys. Rev. 94 (1954) 1111.
[30] L. Szunyogh, B. Ujfalussy, P. Weinberger, Kollár, Phys. Rev. B 49 (1994) 2721.
[31] J. Zabloudil, R. Hammerling, L. Szunyogh, and P. Weinberger, *Electron Scattering in Solid Matter A Theoretical and Computational Treatise*, edited by M. Cardona, P. Fulde, K. von Klitzing, R. Merlin, H.-J. Queisser, H. Störmer, Springer Series in Solid-State Sciences (Springer-Verlag Berlin, 2010).
[32] M. Zwierzycki and O. K. Andersen, Acta Phys. Pol. A 115 (2009) 64.
[33] J. Kollár, L. Vitos, and H. L. Skriver, From ASA Towards the Full Potential. In *Electronic Structure and Physical Properties of Solids: The Uses of the LMTO method* ed. H. Dreyssé, Lectures Notes in Physics **535**, Springer-Verlag Berlin (2000) pp. 85-113.
[34] L. Vitos, J. Kollár, H. L. Skriver, Phys. Rev. B 55 (1997) 4947; Phys. Rev. B 55 (1997) 13521; Phys. Rev. B 55 (1997) 15353.
[35] L. Vitos, J. Kollár, H. L. Skriver, Phys. Rev. B 49 (1994) 11288; Phys. Rev. B 49 (1994) 16694.
[36] L. Vitos, I. A. Abrikosov, and B. Johansson, Phys. Rev. Lett. 87 (2001) 156401.
[37] L. Vitos, P. A. Korzhavyi, and B. Johansson, Phys. Rev. Lett. 88 (2002) 155501; Nature Mater. 2 (2003) 25.
[38] L. Vitos and B. Johansson, Phys. Rev. B 79 (2009) 024415.
[39] A. Taga, L. Vitos, B. Johansson, and G. Grimvall, Phys. Rev. B 71 (2005) 014201.
[40] L. Huang, L. Vitos, S. K. Kwon, B. Johansson, and R. Ahuja, Phys. Rev. B 73 (2006) 104203.
[41] B. Magyari-Köpe, L. Vitos, and G. Grimvall, Phys. Rev. B 70 (2004) 052102.
[42] B. Magyari-Köpe, L. Vitos, B. Johansson, and J. Kollár, Acta Crystallogr., Sect. B: Struct. Sci. 57 (2001) 491.
[43] B. Magyari-Köpe, L. Vitos, B. Johansson, and J. Kollár, J. Geophys. Res. 107 (2002) 2136.

[44] A. Landa, C.-C. Chang, P. N. Kumta, L. Vitos, and I. A. Abrikosov, Solid State Ionics 149 (2002) 209.
[45] B. Magyari-Köpe, L. Vitos, G. Grimvall, B. Johansson, and J. Kollár, Phys. Rev. B 65 (2002) 193107.
[46] E. Wimmer, H. Krakauer, M. Weinert, and A.J. Freeman, Phys. Rev. B 24 (1981) 864.
[47] H. J. Monkhorst and J. D. Pack, Phys. Rev. B 13 (1976) 5188.
[48] C. Kittel. *Introduction to Solid State Physics*, 8th Edition. (Univ. of California, Berkeley, 2005).
[49] A.C. Lawson, A.C. Larson, M.C.Aronson, S. Johnson, Z. Fisk, P.C. Canfield, J.D. Thompson, and R.B. Von Dreele, J. Appl. Phys. 76 (1994) 7049.
[50] M. Ropo, K. Kokko, and L. Vitos Phys. Rev. B 77 (2008) 195445.
[51] M. Aldén, H. L. Skriver, S. Mirbt, and B. Johansson, Phys. Rev. Lett. 69 (1992) 2296.
[52] M. Aldén, H. L. Skriver, S. Mirbt, and B. Johansson, Surface Science 315 (1994) 157.
[53] W.R. Tyson and W.A. Miller, Surf. Sci. 62 (1977) 267.
[54] R.C. Cammarata, Surf. Sci. 279 (1992) 341.
[55] U. K. Poulsen, J. Kollár, and O. K. Andersen, J. Phys. F: Metal Phys. 6 (1976) L241.

Figure 1. Theoretical surface energies for 3*d* metals. For comparison, the theoretical surface energies obtained for the 4*d* (squares) and 5*d* (triangles) series are also shown. Each data corresponds to the thermodynamically stable facets (see Table 3) of the low temperature crystallographic structures: hcp for Sc, Ti, Zn, Co, Y, Zr, Tc, Ru, La, Hf, Re and Os; bcc for V, Fe, Nb, Mo, Ta and W; B2 for Cr; α-Mn; and fcc for Ni, Cu, Rh, Pd, Ag, Ir, Pt and Au.

Figure 2. Comparison between three sets of surface energies calculated for the non-relaxed bcc (001) surface of V, Cr, Mn and Fe using the VASP, EMTO and WIEN2k computer programs. Results are shown for non-magnetic (NM) and magnetic (FM) phases.

Figure 3. Theoretical surface stress for 3*d* metals. For comparison, the theoretical surface stresses obtained for the 4*d* (squares) and 5*d* (triangles) series are also shown. Each data corresponds to the thermodynamically stable facets of the low temperature crystallographic structures (see caption for Figure 2).

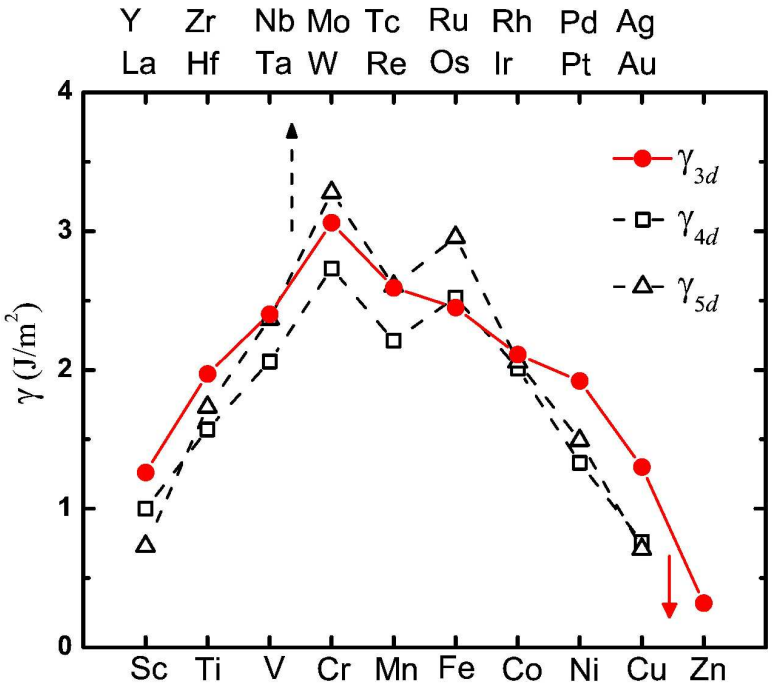

Theoretical surface energies for 3d metals. For comparison, the theoretical surface energies obtained for the 4d (squares) and 5d (triangles) series are also shown. Each data corresponds to the thermodynamically stable facets (see Table III) of the low temperature crystallographic structures: hcp for Sc, Ti, Zn, Co, Y, Zr, Tc, Ru, La, Hf, Re and Os; bcc for V, Fe, Nb, Mo, Ta and W; B2 for Cr; α-Mn; and fcc for Ni, Cu, Rh, Pd, Ag, Ir, Pt and Au.
279x215mm (600 x 600 DPI)

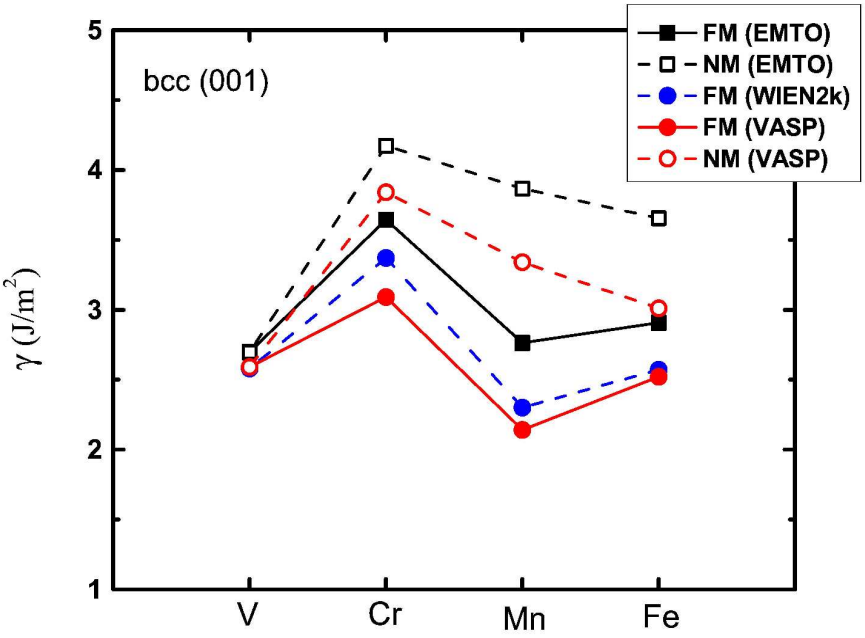

Comparison between three sets of surface energies calculated for the non-relaxed bcc (001) surface of V, Cr, Mn and Fe using the VASP, EMTO and WIEN2k computer programs. Results are shown for non-magnetic (NM) and magnetic (FM) phases.
279x215mm (600 x 600 DPI)

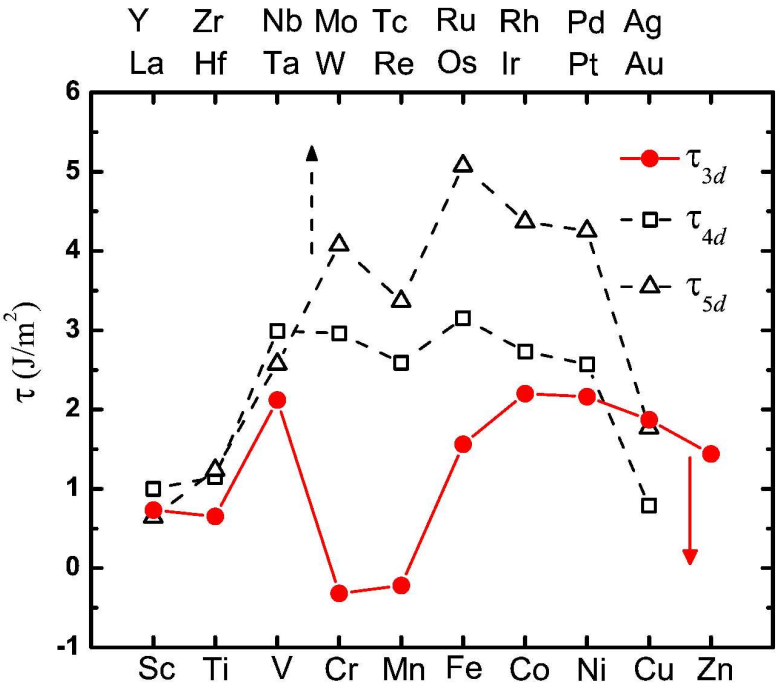

Theoretical surface stress for 3d metals. For comparison, the theoretical surface stresses obtained for the 4d (squares) and 5d (triangles) series are also shown. Each data corresponds to the thermodynamically stable facets of the low temperature crystallographic structures (see caption for Figure 2).
279x215mm (600 x 600 DPI)